J Appl Electrochem (2009) 39:1553–1558
DOI 10.1007/s10800-009-9837-y

ORIGINAL PAPER

Preparation and electrochemical characterization of platinum and ruthenium catalysts deposited on fluorinated carbon supports

Seok Kim · Hee-Jin Sohn · Sung-Kwon Hong · Soo-Jin Park

Received: 17 June 2008 / Accepted: 10 February 2009 / Published online: 18 March 2009

Abstract The effect of fluorination on carbon blacks (CBs) was investigated by analyzing the CB surface functional groups. Also, fluorinated CB supported platinum–ruthenium electrocatalysts were studied. The surface characteristics of the fluorinated CB-supported catalysts were determined by Fourier transform infrared (FT-IR) spectroscopy and X-ray photoelectron spectroscopy (XPS), and their crystallinity was evaluated using X-ray diffraction (XRD). The electrochemical properties of the fluorinated CB-supported platinum and ruthenium (Pt/Ru CBs) catalysts were analyzed by cyclic voltammetry (CV). From the FT-IR results, the introduction of a fluorine atom onto CBs was confirmed by the existence of a carbon–fluorine (C–F) characteristic peak. The XPS result also showed that the fluorine content increased with increasing heat treatment temperature. The XRD analysis revealed that the catalysts are composed of mostly Pt and Ru. This result agreed with the fact that the electrochemical activity of the Pt/Ru CB catalysts was enhanced due to the small size and a high loading of catalysts by surface modification of the CBs.

S. Kim
Department of Chemical Engineering, Pusan National University, San 30, Jangjeon-dong, Geumjeong-gu, Pusan 609-735, Republic of Korea

H.-J. Sohn · S.-K. Hong
Polymer Science and Engineering, Chungnam National University, 220, Yuseong, Daejeon 305-764, Republic of Korea

S.-J. Park (✉)
Department of Chemistry, Inha University, 253, Nam-gu, Incheon 402-751, Republic of Korea
e-mail: sjpark@inha.ac.kr

Keywords Fluorination · Catalysts · Carbon blacks · Carbon supports · Cyclic voltammetry · Electroactivity

1 Introduction

Fuel cells, energy converting devices with a high efficiency and low emissions, have attracted attention over recent decades due to high global energy demand, a movement away from fossil-fuels and concerns about environmental pollution. However, there are many obstacles to be overcome until the Direct Methanol Fuel Cell (DMFC) system can be commercialized as a viable portable power source. One of the reasons is the relatively slow kinetics of the methanol oxidation reaction at an anode, which leads to high over-potentials [1–7]. Pt catalyst is well known as the best material for alcohol oxidation at low temperature. However, pure Pt can easily be poisoned by strongly adsorbed species such as CO-containing materials, which are formed by the initial dehydrogenation of alcohol molecules. To enhance the alcohol-oxidizing activity of Pt catalyst, alloying metals such as Ru, Sn, Mo, Rh or Pb, is used [8–13]. The outstanding performance of Pt/Ru catalysts for the electro-oxidation of H_2 in the presence of CO has been a subject of discussion in recent years [14–18]. On the other hand, in order to exploit the advantageous structural properties of carbon support materials, new types of carbon materials have been used as DMFC-catalyst supports. Electrocatalysts for fuel-cell electrodes are mostly composed of Pt-based metal nanoparticles, which are usually dispersed on porous carbon supports. In order to be suitable for fuel-cell applications, carbon supports should have several characteristics, including a high surface area for finely dispersing catalytic metal particles, high electrical conductivity providing electrical pathways, and mesoporosity for facile diffusion of

reactants and a water handling capability. Recently, carbon blacks, activated carbons, carbon nanofibers, carbon nanotubes, mesoporous carbons and graphitic carbons have all been utilized as catalyst supports for fuel cells [19–28]. Several surface modifications have been applied to carbon materials in order to increase the electrochemical reaction rate and capacity, by using surface oxidation, surface fluorination, and high temperature treatment. In comparison with other surface modification techniques, fluorine atoms can penetrate the material surfaces to relatively great depths depending on treatment conditions [29–31].

In the present study the effects of fluorinated carbon blacks (CBs) on metal–alloy catalysts were investigated by analyzing their surface functional groups. Pt/Ru CBs catalysts were prepared by chemical reduction. The crystallinity and morphology of the catalysts was investigated by X-ray diffraction (XRD) and a transmission electron microscopy (TEM). The electrochemical behavior of the catalysts for methanol electro-oxidation was evaluated by cyclic voltammetry (CV).

2 Experimental

2.1 Materials and preparation of treated CBs

CBs were used as support for the metal catalysts. Chloroplatinic acid (H_2PtCl_4) and ruthenium chloride ($Ru(OH)_3$) catalysts were purchased from Aldrich. The reducing agent, HCHO (35%), was also obtained from Aldrich.

Before catalyst deposition, CBs were exposed to treatment at different temperatures (RT ~ 400 °C) under fluorine gas flow in order to realize their different Pt and Ru loading contents, respectively.

Figure 1 shows a schematic diagram of the fluorination apparatus. The CBs were fluorinated under several conditions. The fluorination reaction was performed under F_2 gas in a batch reactor made of nickel with an outer electric furnace. After evacuation, the fluorine gas was introduced to the reactor at different temperatures, and then the reactive gas was purged from the reactor with nitrogen gas. The fluorination temperatures were varied between room temperature and 400 °C. We considered five carbon samples; pristine CBs, CBs-RT, CBs-100, CBs-300, and CBs-400. The pressure was 0.1 MPa and the nominal reaction time 15 min at the given treatment temperature.

2.2 Preparation of CBs-supported Pt/Ru catalysts

The CB-supported Pt and Ru catalysts were prepared by chemical reduction of Pt/Ru colloids in an aqueous solution using HCHO as a reducing agent. 125 mg of fluorinated CB was suspended in 25 mL of deionized water and stirred ultrasonically for 20 min. Separately, 58.3 mg of H_2PtCl_4 and 30 mg of $Ru(OH)_3$ in dissolved deionized water was slowly added dropwise to the above solution and stirred for 1 h. A 5 M NaOH solution was added to adjust the pH of the solution. Then, HCHO (37%, 0.75 mL) was added to the solution to reduce the Pt and Ru at 85 °C, and an argon-gas flow was passed through the reaction system to isolate oxygen and to remove organic by-products. CB-supported Pt and Ru catalyst powder was filtered and washed with deionized water and ethanol. Then, the powder was dried at 70 °C for 24 h.

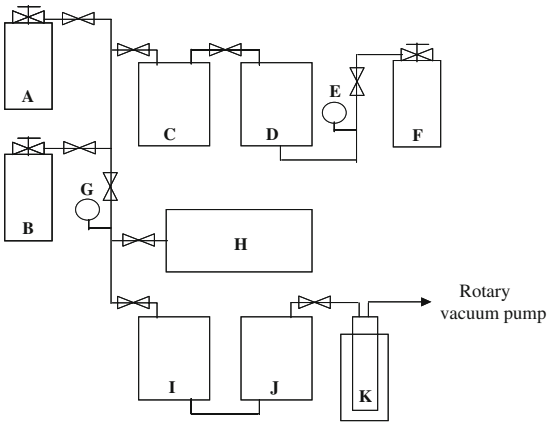

Fig. 1 Schematic diagram of fluorination apparatus. *A* N_2 gas cylinder, *B* O_2 gas cylinder, *C* Buffer tank, *D* F_2 gas tank, *E* Pressure gauge, *F* F_2 gas cylinder, *G* Pressure gauge, *H* reactor, *I* F_2 absorber (Al_2O_3), *J* F_2 absorber (Al_2O_3), *K* Liquid nitrogen

2.3 Characterization methods

The surface modification of the fluorination was confirmed by Fourier transform-IR (FT-IR) spectroscopy (MIDAC, M2000). The scans were performed from 400 to 4000 cm^{-1} and required 40 s to complete. The carbon and fluorine loading level was calculated by energy dispersive X-ray spectroscopy (EDS), considering the atomic ratio of the carbon and fluorine intensity. Transmission electron microscopy (TEM) photographs of the catalyst samples were acquired by 1 nm-spatial-resolution TEM. In the sample preparation for the TEM, the catalyst samples were finely ground and ultrasonically dispersed in isopropyl alcohol, and a drop of the resultant dispersion was deposited and dried on a standard copper-grid coated with a polymer film. The voltage applied to the catalyst was 100 kV. X-Ray diffraction (XRD) analysis with a Rigaku D/MAX-2200 V diffractometer using a Cu Kα ($\lambda = 0.15406$ nm) source operating at 40 kV and 40 mA, was carried out on catalysts from different precursors. The XRD patterns were plotted at a scanning rate of 4° min^{-1} with an angular resolution of 0.05° for the 2θ scan. The X-ray diffractograms were

obtained for 2θ values varying between 10° and 100°. The loading masses of the Pt and Ru were determined using an inductively coupled plasma-atomic emission spectrometer (ICP-AES) using a. Jobin Yvon Ultima C-spectrometer. The samples were also analyzed by X-ray photoelectron spectroscopy (XPS) on a VG Scientific LAB MK-II spectrometer. The pressure in the sample chamber was controlled in the range 10^{-8} to 10^{-9} Torr.

2.4 Electrochemical measurements

Electrochemical measurements were carried out in a conventional three-electrode electrochemical cell at 25 °C. A piece of Pt wire was used as a counter electrode, and KCl-saturated Ag/AgCl was used as reference electrode. The working electrode, a glassy carbon electrode, was covered with catalyst powder. All the solutions were prepared with ultra-pure water. A solution of 1 M CH_3OH and 0.5 M H_2SO_4 was stirred constantly and purged with ultra-pure argon gas. Electrochemical experiments were performed using Autolab with PGSTAT 30, an electrochemical analysis instrument. The potential was changed linearly from −0.2 to 0.8 V vs. Ag/AgCl. The potential scan rate was 10 mV s^{-1}.

3 Results and discussion

3.1 Surface characteristics and chemical structure analyses

FT-IR spectroscopy was employed to analyze the functional groups of the fluorinated CBs surface, as shown in Fig. 2. The fluorinated CBs showed characteristic peaks for the fluorine incorporated into the surface during fluorination; peaks are observed as C–F groups at 1400–1000 cm^{-1}. In the case of the fluorinated CBs, the band intensity at 1400–1000 cm^{-1} was increased with fluorination temperature, due to changes in the functional groups. The band intensity of the pristine CBs at 1400–1000 cm^{-1} was rather weaker than that of the fluorinated CBs. The peaks are typical bands that are assigned to a very small amount of moisture (OH) and CO_2 in air at $\sim$3400 cm^{-1} and 1630 cm^{-1} respectively. These peak intensities were increased because the treatment was intensified with increasing temperature. Elemental analysis of the fluorinated CBs is listed in Table 1. The fluorine contents were relatively higher in the heat-treated CBs, in particular in the sample fluorinated at 400 °C. The fluorine content was 4.68% for the CBs fluorinated at 400 °C. This suggests that the fluorine contents increased with increasing heat-treatment temperature, probably due to the active radicals of fluorine atoms produced on the edge planes of the CBs. This result would probably lead to an improvement in the electrochemical properties of Pt/Ru CBs, owing to an increase in specific polarity and the formation of fluorine bonding in the CBs.

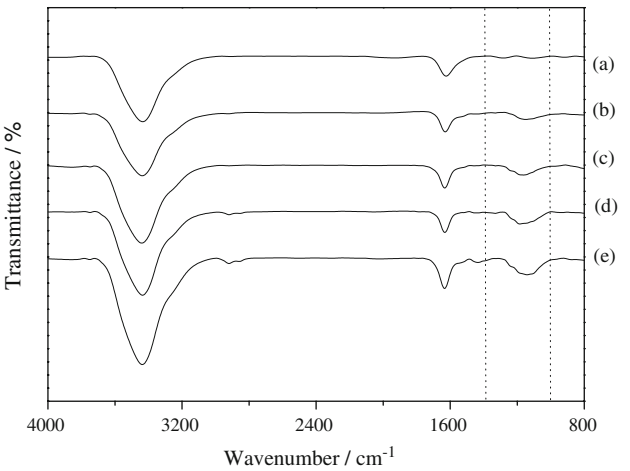

Fig. 2 FT-IR spectra of Pt/Ru CBs: (a) pristine CBs (b) CBs-RT (c) CBs-100 (d) CBs-300 (e) CBs-400

Table 1 Elemental contents of fluorinated CBs as measured by EDS

Sample	Carbon (wt.%)	Fluorine (wt.%)
Pristine CBs	97.59	0
CBs-RT	96.92	1.82
CBs-100	96.02	2.59
CBs-300	95.62	3.97
CBs-400	93.83	4.68

The nature of the surface species of the prepared Pt/Ru CBs samples was investigated by XPS analysis. Figure 3 shows the XPS survey scan spectra for the 0–1100 eV binding energies before (a) and after (b)–(d) fluorination (RT-400 °C). The survey spectra for the Pt/Ru CBs confirmed the near-surface presence of C, Pt, Ru and F (with binding energies of 281.7, 69.7, 459, and 684 eV, respectively) characteristic peaks. From the XPS spectra, the surface composition for CB-400 shows a Pt loading of 15% and a Ru loading of 6.34%. The Pt and Ru contents of the Pt/Ru CBs increased with increasing fluorination temperature, probably due to the increase in the number of fluorine-containing CB groups after fluorination.

3.2 Physical properties

The crystalline structures of the Pt/Ru CBs catalysts prepared at various fluorination temperatures were investigated by XRD. Figure 4 shows the XRD patterns. The diffraction peak at 25° in all the XRD patterns of the carbon-supported catalysts is due to the (002) plane of the hexagonal structure of carbon. The diffraction peaks at 40, 46, 67, and 81° represent the (111), (200), (220), and (311) planes of the face-centered cubic (fcc) structure, respectively. The XRD

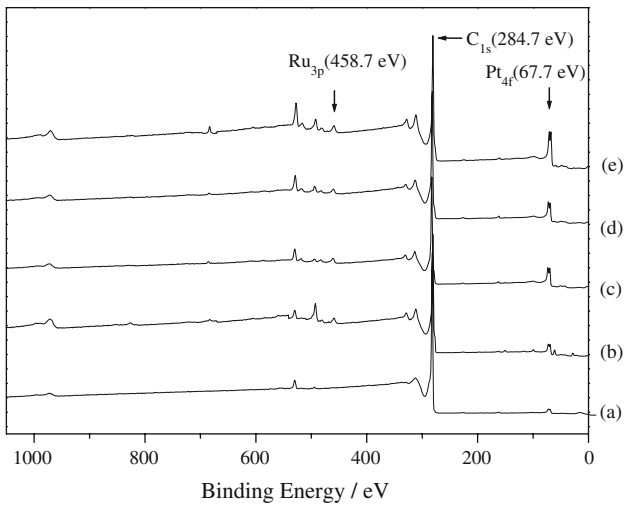

Fig. 3 XPS spectra of Pt/Ru CBs: (a) pristine CBs (b) CBs-RT (c) CBs-100 (d) CBs-300 (e) CBs-400

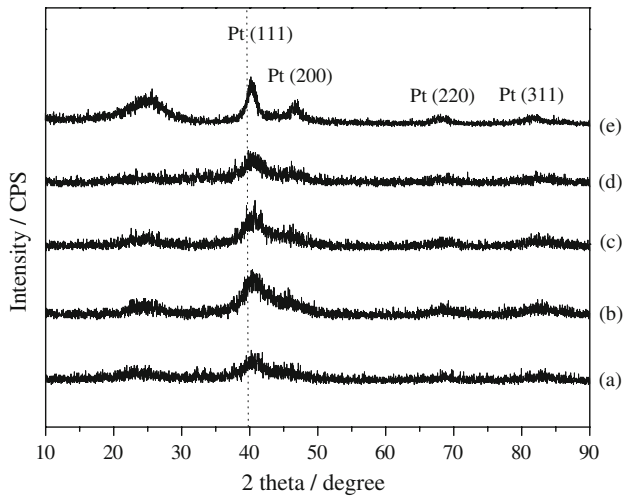

Fig. 4 XRD spectra of Pt/Ru CBs: (a) pristine CBs (b) CBs-RT (c) CBs-100 (d) CBs-300 (e) CBs-400

analysis showed sharper and more intense diffraction peaks. The fluorination treatment generally produced an increase in crystallinity. All the catalysts showed diffraction patterns similar to that of Pt itself. The 2θ values of the (111) peak for Pt/Ru CBs catalysts were shifted to slightly higher angles with slightly different amounts compared with that of pure Pt (39.9°) represented by the vertical dotted line. The high angle shift of the main peaks is indicative of good alloy formation of PtRu nanoparticles regardless of the supporting materials used.

The loading efficiencies of Pt and Ru were measured by the ICP-AES method, and the results are listed in Table 2. The fluorinated CBs at 400 °C showed the highest value, 12.6% (at Pt) and 5.81% (at Ru), whereas the as-received CBs showed the lowest value, 4.74% (at Pt) and 1.1% (at Ru), indicating clearly that in the case of fluorinated CBs, the CB surface Pt and Ru loading contents were enhanced.

Table 2 Average particle size and elemental contents of fluorinated Pt/Ru CBs

Sample	Platinum (wt.%)[b]	Ruthenium (wt.%)[b]	Particle size (nm)[a]
Pristine CBs	4.74	1.10	3.84
CBs-RT	7.05	2.81	2.98
CBs-100	9.50	3.75	2.85
CBs-300	10.90	4.04	2.53
CBs-400	12.60	5.81	2.10

[a] Estimated from TEM

[b] Estimated from ICP-AES

The morphologies and particle-size distributions of the Pt/Ru CBs catalysts were investigated by TEM. The results are shown in Fig. 5. The Pt–Ru particles were distributed uniformly and with high dispersion on the CB support. Many catalyst nanoparticles of about 2–3 nm diameter are uniformly spread over the surface. It is well-known that the good dispersion of metal nanoparticles on the support can lead to excellent methanol oxidation activity at the surfaces of metal/carbon catalysts [29]. The average sizes of the alloy particles are summarized in Table 2. They decreased from 3.84 to 2.10 nm as a function of fluorination temperature, and the smallest was found in the CB fluorinated at 400 °C, indicating that the average particle size of metallic alloys could be controllable in this system.

3.3 Electrochemical properties of catalysts

CVs of the Pt/Ru CBs catalysts were obtained in 1.0 M of CH_3OH + 0.5 M of H_2SO_4 aqueous solution. Figure 6 shows representative voltammograms of the Pt/Ru CBs catalysts. It was shown that the upper potential limit had an important effect on the stability of Ru in the Pt/Ru CB catalysts. To avoid leaching of Ru, the upper limit for the catalysts was set to 0.8 V. It can be seen that the methanol oxidation activity in the Pt/Ru CB catalysts varied with electrode potential. The voltammetric behavior was found to be dependent on Pt content.

Figure 7 shows the electrocatalytic mass activities for each sample, that is, electrocatalytic currents per gram of Pt, measured at 650 mV. When the fluorination temperature was increased to 400 °C, the specific current density gradually increased to 192.53 mA mg^{-1}. Consequently, the electrochemical activity was increased with increasing fluorination temperature, the maximum being found at 400 °C. The Pt content on the support was found to be the highest for the CB-400 sample. The Pt/Ru CB catalysts showed an average size of 2–3 nm. From this result, it may

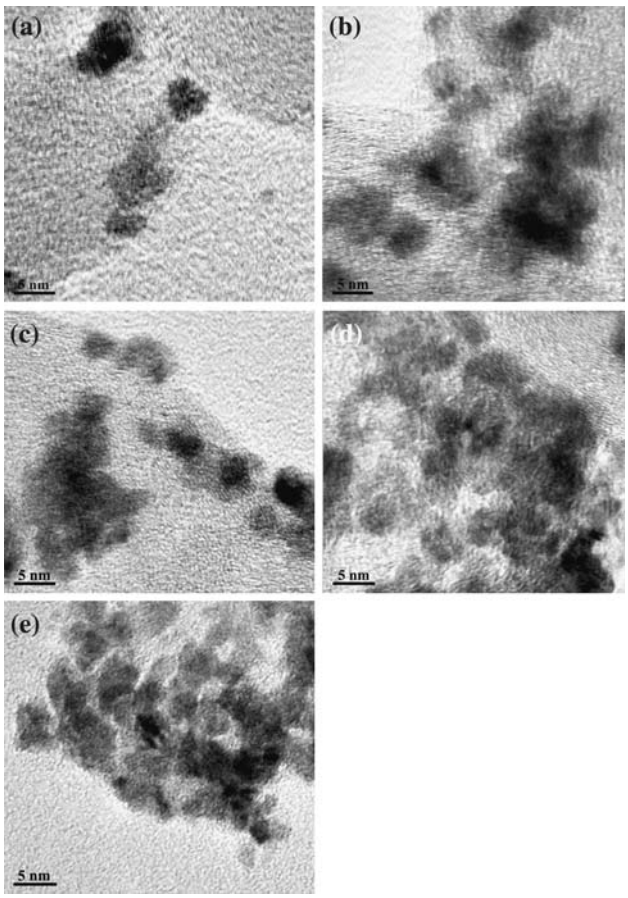

Fig. 5 TEM micrograph of Pt/Ru CBs: **a** pristine CBs **b** CBs-RT **c** CBs-100 **d** CBs-300 **e** CBs-400

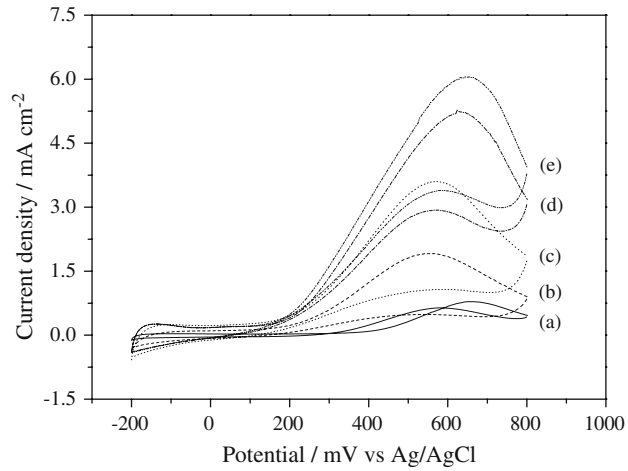

Fig. 6 Cyclo voltammograms of fluorinated Pt/Ru CBs in 0.5 M of H_2SO_4 + 1.0 M of CH_3OH: (a) pristine CBs (b) CBs-RT (c) CBs-100 (d) CBs-300 (e) CBs-400

be concluded that small metal particles and high catalyst loading leads to an increase in the active areas, resulting in good electrocatalytic properties for methanol oxidation.

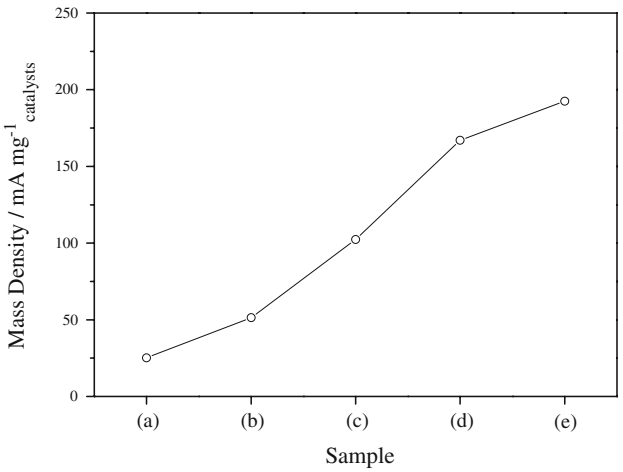

Fig. 7 Catalytic activity of Pt measured at a potential of +650 mV for CV results of Pt/Ru CBs: (a) pristine CBs (b) CBs-RT (c) CBs-100 (d) CBs-300 (e) CBs-400

4 Conclusions

The effects of fluorinated CBs on metal–alloy catalysts were investigated by analyzing the functional groups of the CBs. It was found that high electrochemical catalytic activity was a function of alloy catalyst formation, surface modification and chemical composition of the catalyst. As a result of thermal treatment in fluorine gas, the alloy nanoparticles were highly dispersed over the CB surface, the size of the particles being decreased. The nanoparticle sizes of the Pt/Ru CB catalysts could be controlled in the range 2–3 nm by the fluorination temperature. The electrochemical activity increased with increasing fluorination temperature; the maximum occurring at 400 °C. It was found that the optimal fluorination temperature for electrochemical activity of catalyst was 400 °C. Pt/Ru CB catalysts prepared from fluorinated CB showed higher electrocatalytic activity for methanol oxidation than non-fluorinated CBs.

Acknowledgement This work was carried out for the Hydrogen Energy R&D Center, one of the 21st Century Frontier R&D Program, funded by the Ministry of Science and Technology of Korea.

References

1. Arava LMR, Natarajan R, Sundara R (2008) Carbon 46:2
2. Pinto LMC, Silva ER, Caram R, Tremiliosi-Filho G, Angelo ACD (2008) Intermetallics 16:246
3. Kim S, Park SJ (2006) J Power Sources 159:42
4. Okawa Y, Hirata Y (2005) J Eur Ceram Soc 25:473
5. Jeon MK, Won JY, Oh KS, Lee KR, Woo SI (2007) Electrochim Acta 53:447
6. Zhou WJ, Song SQ, Li WZ, Sun GQ, Xin Q, Kontou S, Poulianitis K, Tsiakaras P (2004) Solid State Ion 175:797

7. Joo SH, Pak C, You DJ, Lee SA, Lee HI, Kim JM, Chang H, Seung DY (2006) Electrochim Acta 52:1618
8. Kimberly M, Mcgrath GK, Prakash S, Olah GA (2004) J Ind Eng Chem 10:1063
9. Statti P, Poltarzewski Z, Alderucci V, Maggio G, Giordano N (1994) Int J Hydrogen Energy 19:523
10. Hall SC, Subramanian V, Teeter G, Rambabu B (2004) Solid State Ion 175:809
11. Wang H, Jusys Z, Behm RJ (2006) J Power Sources 154:351
12. Delime F, Leger JM, Lamy C (1999) J Appl Electrochem 29:1249
13. Li GC, Pickup PG (2006) Electrochim Acta 52:1033
14. Jung YJ, Kim S, Park SJ, Kim JM (2008) Colloids Surf A Physicochem Eng Asp 313–314:167
15. Bessel CA, Laubernds K, Rodriguez NM, Baker RTK (2001) J Phys Chem B 105:1115
16. Ueda S, Eguchi M, Uno K, Tsutsumi Y, Ogawa N (2006) Solid State Ionics 177:175
17. Chai GS, Yoon SB, Yu JS, Choi JH, Sung YE (2004) J Phys Chem B 108:7074
18. Lin Y, Cui X, Yen C, Wai CM (2005) J Phys Chem B 109:14410
19. Lee JS, Quan ND, Hwang JM, Lee SD, Kim HG, Lee HJ, Kim HS (2006) J Ind Eng Chem 12:175
20. Kim S, Park SJ (2007) J Solid State Electrochem 11:821
21. Kim S, Park (2007) Electrochim Acta 52:3013
22. Kim S, Jung YJ, Park SJ (2008) Colloids Surf A Physicochem Eng Asp 189:313–314
23. Hyeon T, Han S, Sung YE, Park KW, Kim YW (2003) Angew Chem Int Edit 42:4352
24. Park KW, Sung YE, Han S, Yun Y, Hyeon T (2004) J Phys Chem B 108:929
25. Joo SH, Choi SJ, Oh I, Kwak J, Liu Z, Terasaki O, Ryoo R (2001) Nature 412:169
26. Ding J, Chan KY, Ren J, Xiao FS (2005) Electrochim Acta 50:3131
27. Su F, Zeng J, Bao X, Yu Y, Lee JY, Zhao XS (2005) Chem Mater 17:3960
28. Nam JH, Jang YY, Kwon YU, Nam JD (2004) Electrochem Commun 6:737
29. Liu Z, Ling XY, Guo B, Hong L, Lee JY (2007) J Power Sources 167:272
30. Nakajima T, Gupta V, Ohzawa Y, Koh M, Singh RN, Tressaud A, Durand E (2002) J Power Sources 104:108
31. Nakajima T (2007) J Fluor Chem 128:277